IEEE Access
Multidisciplinary | Rapid Review | Open Access Journal

Received November 4, 2018, accepted November 13, 2018, date of publication November 29, 2018,
date of current version December 27, 2018.

Digital Object Identifier 10.1109/ACCESS.2018.2883492

The Coordinated Control of Wind-Diesel Hybrid Micro-Grid Based on Sliding Mode Method and Load Estimation

MINGHAN YUAN[1], YANG FU[1,2], YANG MI[2], ZHENKUN LI[2], AND CHENGSHAN WANG[3]
[1]School of Mechatronic Engineering and Automation, Shanghai University, Shanghai 200444, China
[2]Electrical Engineering Department, Shanghai University of Electric Power, Shanghai 200090, China
[3]The Key Laboratory of Smart Grid, Ministry of Education, Tianjin 300072, China

Corresponding author: Yang Fu (mfudong@126.com)

This work was supported in part by the National Natural Science Foundation of China under Grant 61873159, in part by the Shanghai Committee of Science and Technology under Project 18020500700, in part by Electrical Engineering Shanghai Class II Plateau Discipline, and in part by the Shanghai Green Energy Grid Connected Technology Engineering Research Center under Grant 13DZ2251900.

ABSTRACT In order to reduce the frequency deviation resulting from renewable energy fluctuation and load variance, the coordination control strategy for isolated wind-diesel hybrid micro-grid is proposed by taking advantage of smart neural network observer and sliding mode method. For diesel generator system side, the sliding mode load frequency control including load variance is designed to regulate the output power. For the wind turbine generator system side, the sliding mode pitch angle control considering load variance is constructed to smooth the wind turbine generator output power fluctuation. Furthermore, the different coordinated strategies are proposed to realize the plug and play for the hybrid micro-grid, it is easy to see that the control accuracy can be improved by the designed neural network adaptive observer and considering the load variation. The effectiveness of the proposed control strategy is validated through real time digital simulator platform under different operation condition.

INDEX TERMS Observer, frequency control, isolated micro-grid, wind-diesel system, sliding mode.

I. INTRODUCTION

Power supply is difficult for remote area and island due to traffic inconvenience, but these areas always have plentiful wind energy [1]–[3] which can be fully exploited for its clean, rich and renewable characteristic. Because the wind power is fluctuated, so the hybrid micro-grid is an effective multi energy complementary power supply mode. Furthermore, in order to assure the micro-grid stability operation, the wind turbine generator (WTG) system side and the diesel generator (DG) system side need to be equipped with advanced control strategy together [4]–[6].

The different pitch angle controllers are designed to smooth the WTG output power [1]–[5]. The proportional-integral (PI) pitch angle control (PAC) is designed to smooth the wind fluctuation power, which can reduce the frequency deviation of the micro-grid through the WTG output power regulation in [1]. In [2] and [3], the fuzzy PI pitch angle control is designed to control WTG output power. In [4], the proportional-integral-differential (PID) neural network controller is designed to regulate blade pitch angle and keep the stable power output. The sliding mode (SM) pitch angle control is designed for wind turbine which can improve the control system robustness in [5]. The different optimization methods can improve the pitch angle control effectively and smooth the output power of WTG. However, in order to reduce the frequency deviation in the micro-grid, only the WTG pitch angle control design is not enough.

Considering the load variance in the hybrid micro-grid, the load frequency control (LFC) is designed for the diesel system to reduce the frequency deviation [6]. The traditional LFC is often designed by using PID method [7]–[9]. The other modern control methods in LFC [10]–[15] have also been proposed such as fuzzy logic, internal model control, adaptive control, neural network, SM algorithm and so on. Especially, SM algorithm is utilized widely to design the controller because of its strong robustness. In [14], the decentralized SM LFC is designed for multi-area power system with parameter perturbation, the frequency deviation is attenuated according to the load changes and different operation condition, but the renewable energy is not considered. In [15],

the third order SM observer-based approach is proposed for optimal LFC in power networks with partition control.

The above studies may optimize the PAC of WTG and LFC of diesel system respectively. In order to further improve the frequency regulation, the energy storage system is applied to smooth frequency fluctuation in [16]–[18], but the operation cost may increase accordingly. In [19], the modified hierarchical coordinated control method is applied to reduce the frequency deviation by utilizing the kinetic energy of WTG and DG. However, the disturbance of source and load is not considered.

Based on the analysis, the novel coordinated control strategy is presented for isolated hybrid micro-grid including source and load disturbance. Furthermore, in order to compensate load fluctuation and improve the control accuracy, the SM pitch angle control is constructed to regulate WTG output power with frequency signal compensation, and the SM LFC based on neural network adaptive disturbance observer is designed for DG system. The proposed control strategy cannot only adjust the WTG output power according to the dynamic reference, but also reduce the frequency deviation and improve the control accuracy through the designed disturbance observer.

The rest of this paper is organized as follows. The isolated hybrid micro-grid model is constructed in section II. In section III, the SM pitch angle control of WTG system and SM LFC of diesel generator system are designed by using neural network adaptive disturbance observer. The proposed coordinated control strategy is discussed in section IV. Next section V shows the Real Time Digital Simulator (RTDS) results under different operation cases. Finally, the contribution is summarized and the conclusion is drawn in Section VI.

II. MODEL OF ISOLATED HYBRID MICRO-GRID

The typical isolated hybrid micro-grid is used to design the coordination control strategy which is composed of WTG system, diesel generator system and load. The isolated hybrid micro-grid topological structure diagram is shown as Fig. 1. where P_d is output power of DG system, V_w is wind speed, P_g is output power of WTG system, P_L is load demand power, $\hat{P}_L$ is estimated value, PAC is abbreviation of pitch angle control, radial basis function neural network adaptive observer (RBF NNAO) is about radial basis function neural network adaptive observer.

A. MODEL OF DG

The DG LFC mathematical model [20]–[22] is established by the following equation

$$\Delta\dot{f}(t) = -\frac{1}{T_p}\Delta f(t) + \frac{K_p}{T_p}\Delta P_d(t) - \frac{K_p}{T_p}\Delta P_L(t) \tag{1}$$

$$\Delta\dot{P}_d(t) = -\frac{1}{T_t}\Delta P_d(t) + \frac{1}{T_t}\Delta X_d(t) \tag{2}$$

$$\Delta\dot{X}_d(t) = -\frac{1}{R_{tr}T_g}\Delta f(t) + \frac{1}{T_g}(\Delta X_d(t) - \Delta E(t) + u(t)) \tag{3}$$

$$\Delta\dot{E}(t) = K_E\Delta f(t) \tag{4}$$

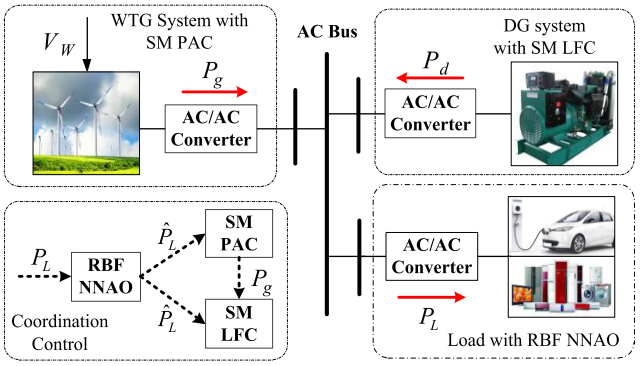

FIGURE 1. The structure diagram of isolated hybrid micro-grid.

where $\Delta f(t)$ is incremental frequency deviation, $\Delta P_d(t)$ is incremental change in DG output power, $\Delta P_L(t)$ is load variation, $\Delta X_d(t)$ is incremental change in governor valve position, $\Delta E(t)$ is incremental change in integral control, T_g is governor time constant, T_t is DG time constant, T_p is power system time constant, K_p is power system gain, R_{tr} is governor speed adjustment coefficient, K_E is integral control gain, $u(t)$ is the designed SM LFC.

The model (1)-(4) can be established as state equation

$$\dot{x}(t) = Ax(t) + Bu(t) + Hd(t) \tag{5}$$

where

$$x = \left[\Delta f(t) \;\; \Delta X_d(t) \;\; \Delta P_d(t) \;\; \Delta E(t)\right]^T, \quad d(t) = \Delta P_L,$$

$$A = \begin{bmatrix} -\frac{1}{T_p} & \frac{K_p}{T_p} & 0 & 0 \\ 0 & -\frac{1}{T_t} & \frac{1}{T_t} & 0 \\ -\frac{1}{R_{tr}T_g} & 0 & -\frac{1}{T_g} & -\frac{1}{T_g} \\ K_E & 0 & 0 & 0 \end{bmatrix}, \quad B = \begin{bmatrix} 0 \\ 0 \\ \frac{1}{T_g} \\ 0 \end{bmatrix},$$

$$H = \begin{bmatrix} -\frac{K_p}{T_p} \\ 0 \\ 0 \\ 0 \end{bmatrix}.$$

B. MODEL OF WTG

The Windmill output power P_w is proportional to the cube of wind speed [23]–[26], which is denoted as

$$P_w = 0.5C_p(\lambda, \beta)V_w^3\rho\pi R^2 \tag{6}$$

where ρ is air density, R is the radius of the windmill, $C_p(\lambda, \beta)$ is the power coefficient, β is the pitch angle, $\lambda = \omega R/V_w$ is the tip-speed ratio, the angular rotor speed ω [23] is as

$$\omega^2 = \int \frac{2}{J}(P_w - P_g)dt \tag{7}$$

where J is moment of inertia for the windmill. Since generator is connected with windmill, which has large inertia,

electric transient is disregarded. Then, the output power P_g of generator [23], [24] can be described as

$$P_g = \frac{-3V_p^2 s(1+s)R_2}{(R_2 - sR_1)^2 + s^2(X_1 + X_2)^2} \tag{8}$$

where V_p is phase voltage, R_1 is stator resistance, R_2 is rotor resistance, X_1 is stator reactance, and X_2 is rotor reactance, $s = (\omega_0 - \omega/\omega_0)$ is the slip of generator, ω_0 is synchronous angular speed. Equations (6)-(8) are the basic configuration [23] of the WTG.

III. CONTROL SYSTEM DESIGN

The SM method is widely used for power system control design because of its robustness, quick response and convenient calculation for engineering application. Here, the SM algorithm is applied to design PAC and LFC. Furthermore, the RBF NNAO is designed to improve the SM LFC and SM PAC precision by using the disturbance estimation.

A. SM LFC DESIGN FOR DG SYSTEM BASED ON RBF NNAO

In the hybrid micro-grid, the DG is controllable power source, so the SM LFC is designed to adjust the output power, which can reduce the frequency deviation due to the load and renewable source disturbance. In order to improve the SM LFC precision, the RBF adaptive disturbance observer is designed to estimate the load disturbance.

The SM LFC design is also divided into two steps. Because the load variation is unknown, so (5) can be rewritten as

$$\dot{x}(t) = Ax(t) + Bu(t) + f(t) \tag{9}$$

where $f(t) = Hd(t)$.

The switching function η_1 is selected as $\eta_1 = c_1 x$, where switching gain matrix c_1 is designed through pole assignment. Define the equivalent control as variable u_{eq}, which can be solved through equation $\dot{\eta}_1 = 0$ together with equation (9) as

$$u_{eq}(t) = -(c_1 B)^{-1}[c_1 Ax(t) + c_1 f(t)] \tag{10}$$

Substitute (10) into (9), the equivalent control equation is given as

$$\dot{x}(t) = \tilde{A}x(t) + \tilde{f}(t) \tag{11}$$

where $\tilde{A} = (I_n - B(c_1B)^{-1}c_1)A$ and $\tilde{f} = (I_n - B(c_1B)^{-1}c_1)f(t)$.

For equilibrium point $x_e = 0$ of linear time invariant system $\dot{x} = \tilde{A}x$, there exists positive definite matrix P which is the solution of the Lyapunov matrix equation $PA + A^T P = -Q$ for any positive definite matrix Q.

The assumption and theorem is proposed to assure the stability of (11).

Assumption, The system uncertainty in (11) satisfies $\left\|\tilde{f}(t)\right\| \leq \|\beta_1(t)\|$, where $\beta_1(t)$ is positive function, $\|*\|$ is Euclidean norm.

Theorem 1: When the assumption holds, for any variable $x \in B_c(\eta)$, the system (11) is stable at any time, where $B_c(\eta)$ is the complement of the closed ball centered at $x = 0$ with radius $\eta = (2\beta_1(t)\|P\|)/\lambda_{\min}(Q_i)$.

Proof: Select the Lyapunov function $v(t)$ as following,

$$v(t) = x^T(t)Px(t) \tag{12}$$

Take derivative of (12) together with (11), and use assumption and theorem condition,

$$\dot{v}(t) \leq -\lambda_{\min}(Q)\|x(t)\|^2 + 2\beta_1(t)\|P\|\|x(t)\| \tag{13}$$

So the equivalent control system is stable for $x \in B_c(\eta)$ at any time.

The SM LFC is designed by using the reaching law as

$$\dot{\eta}_1 = c_1\dot{x} = -\varepsilon_1 sgn(\eta_1)\varepsilon_1 > 0 \tag{14}$$

where ε_1 is positive constant. It is obvious that the hitting condition $\dot{\eta}_1\eta_1 \leq 0$ can be assured. The control law is deduced by (14) as

$$u_d(t) = -(c_1B)^{-1}[c_1Ax(t) + c_1f(t) + \varepsilon_1 sgn(\eta_1)] \tag{15}$$

The load disturbance $f(t)$ in (15) can be estimated by the designed RBF NNAO [27] which improves LFC precision.

According the state equation (9) together with the system output model, the system is extended as

$$\begin{cases} \dot{x}(t) = Ax(t) + Bu(t) + f(t) \\ y(t) = Dx(t) \end{cases} \tag{16}$$

where $D = [1, 0, 0, 0]^T$, u is input, y is output. The system (16) is observable because the matrix $[D, A]$ is full rank.

The load disturbance $f(t)$ can be approximated by the designed three layers RBF neural networks as

$$f(t) = W^T\sigma(x) + \tau(x) \tag{17}$$

where $\sigma(x)$ is gauss function, W is the weight matrix between the hidden layer and output layer of RBF neural network, $\tau(x)$ is approximation error. The estimated value $\hat{f}(t)$ is approximately expressed as $\hat{f}(t) = \hat{W}^T\sigma(\hat{x})$.

The NNAO can be designed as

$$\begin{cases} \dot{\hat{x}}(t) = A\hat{x}(t) + Bu(t) + \hat{W}^T\sigma(\hat{x}) + L(\hat{y}(t) - D\hat{x}(t)) \\ \hat{y}(t) = D\hat{x}(t) \end{cases} \tag{18}$$

where L is gain matrix of observer, $\hat{y}$ is NNAO output.

Define state error $\tilde{x}(t) = x(t) - \hat{x}(t)$ and output error $\tilde{y}(t) = y(t) - \hat{y}(t)$, gauss function error $\sigma(x, \hat{x}) = \sigma(x) - \sigma(\hat{x})$. According to (16)-(18), the error system can be described as

$$\begin{cases} \dot{\tilde{x}}(t) = A_L\tilde{x}(t) + \tilde{W}^T\sigma(\hat{x}) + \theta(x) \\ \tilde{y}(t) = D\tilde{x}(t) \end{cases} \tag{19}$$

where $\tilde{W} = W - \hat{W}$, $A_L = A - LD$ is an asymptotically stable Hurwitz matrix, $\theta(x) = W^T\sigma(x, \hat{x}) + \tau(x)$is bounded disturbance and it satisfies $\|\theta(x)\| \leq \bar{\xi}$, $\bar{\xi}$ is a positive constant.

In order to prove the error system stability, (19) can be transformed as

$$s\tilde{x}(s) = A_L\tilde{x}(s) + \tilde{W}\sigma(\hat{x}) + \theta(x) \tag{20}$$

Then

$$\tilde{y}(s) = H(s)(\tilde{W}\sigma(\hat{x}) + \theta(x)) \tag{21}$$

where $H(s) = \frac{D^T}{sI - A_L}$ is transfer function and strictly positive real function.

Define $\bar{\theta}(x) = L^{-1}(s)\theta(x)$, $L^{-1}(s)$ as transfer function with stable poles, $\delta(t) = L^{-1}(s)\tilde{W}\sigma(\hat{x}) - \tilde{W}^T L^{-1}(s)\sigma(\hat{x})$, $\|\delta(t)\| \leq c_r \left\|\tilde{W}\right\|_F$, c_r is positive number. The (21) becomes

$$\tilde{y}(s) = H(s)L(s)(\delta(t) + \bar{\theta}(x) + \tilde{W}^T L^{-1}(s)\sigma(\hat{x})) \tag{22}$$

Select $H(s)L(s) = C_c^T(sI - A_c)^{-1}b_c$, $C_c = [1, 0, 0, 0]^T$, $\tilde{y} = C_c\tilde{z}$, then (22) can be expressed as

$$\dot{\tilde{z}} = A_c\tilde{z} + b_c(L^{-1}(s)\tilde{W}\sigma(\hat{x}) + \bar{\theta}(x)) \tag{23}$$

where $A_c \in R^{n\times n}$.

The stability of (23) can be assured by the Theorem 2.

Theorem 2: The observer error system (23) is stable if the two conditions $|\tilde{y}| > (2\bar{\xi} - \frac{1}{2}k_1a_1^2)/\lambda_{\min}(Q)$ and $\left\|\tilde{W}\right\|_F \geq \sqrt{(a_1^2/4 + \bar{\xi}/k_1)} + (1/2)a_1$ must be satisfied together with the designed adaptive law of RBF neural network is

$$\dot{\hat{W}} = F_1\widehat{\bar{\sigma}}\tilde{y} - k_1F_1\,|\tilde{y}|\,\hat{W} \tag{24}$$

where $\widehat{\bar{\sigma}} = L^{-1}(s)\hat{\sigma}$.

Proof: Define Lyapunov function as

$$V = \frac{1}{2}\tilde{z}^T P_1\tilde{z} + \frac{1}{2}tr(\tilde{W}^T F_1\tilde{W}) \tag{25}$$

The derivative of (25) is deduced as

$$\begin{aligned}\dot{V} &= \frac{1}{2}\dot{\tilde{z}}^T P_1\tilde{z} + \frac{1}{2}\tilde{z}^T P_1\dot{\tilde{z}} + tr(\tilde{W}^T F_1^{-1}\dot{\tilde{W}}) \\ &= -\frac{1}{2}\tilde{z}^T Q_1\tilde{z} + \tilde{y}\Delta + tr(\tilde{W}^T F_1^{-1}\dot{\tilde{W}})\end{aligned} \tag{26}$$

where $\Delta = L^{-1}(s)\tilde{W}\sigma(\hat{x}) + \bar{\theta}(x)$.

Substitute the adaptive law (24) into (26), according to the definition of trace, $tr(\tilde{W}^T\widehat{\bar{\sigma}}\tilde{y}) = \tilde{y}\tilde{W}^T\widehat{\bar{\sigma}}$, and $\|\tilde{z}\| \geq |\tilde{y}|$, the (26) can be described as

$$\begin{aligned}\dot{V} &= -\frac{1}{2}\tilde{z}^T Q_1\tilde{z} + \tilde{y}\Delta + tr(\tilde{W}^T F_1^{-1}(-F_1\widehat{\bar{\sigma}}\tilde{y} + k_1F_1\,|\tilde{y}|\,\hat{W})) \\ &= -\frac{1}{2}\tilde{z}^T Q_1\tilde{z} + \tilde{y}(\tilde{W}^T\bar{\sigma} + \delta(t) + \bar{\theta}(x)) - \tilde{y}\tilde{W}^T\widehat{\bar{\sigma}} \\ &\quad + tr(\tilde{W}^T k_1\,|\tilde{y}|\,\hat{W}) \\ &\leq -\frac{1}{2}\lambda_{\min}(Q)\,\|\tilde{z}\|^2 + |\tilde{y}|\,(c_r\left\|\tilde{W}\right\|_F + \bar{\xi}) \\ &\quad + k_1\,|\tilde{y}|\,(W_M\left\|\tilde{W}\right\|_F - \left\|\tilde{W}\right\|_F^2) \\ &= -|\tilde{y}|\,[\frac{1}{4}\lambda_{\min}(Q_1)\,|\tilde{y}| + \frac{1}{4}\lambda_{\min}(Q_1)\,|\tilde{y}| - \bar{\xi} \\ &\quad + k_1(\left\|\tilde{W}\right\|_F - \frac{1}{2}a_1)^2 - \frac{1}{4}k_1a_1^2]\end{aligned} \tag{27}$$

So $\dot{V} < 0$ as $a_1 = W_M + c_r/k_1$. The stability of (23) can be assured. The disturbance in (16) can be replaced by the estimation $\hat{d}(t)$, the improved control law is given as

$$u_D(t) = -(c_1B)^{-1}[c_1Ax(t) + c_1H\hat{d}(t) + \varepsilon_1 sgn(\eta_1)] \tag{28}$$

B. SM PAC DESIGN FOR WTG

Considering the WTG output power participation, u_w is defined as the compensated control input of PAC, so equation (1) can be rewritten as

$$\Delta\dot{f}(t) = -\frac{1}{T_p}\Delta f(t) + \frac{K_p}{T_p}(\Delta P_d(t) - \Delta P_L(t) + u_W) \tag{29}$$

The model (2)-(4) and (29) can be established as

$$\dot{x}(t) = Ax(t) + B_1u_W(t) + f(t) \tag{30}$$

where $B_1 = [\,\frac{K_P}{T_P}\ 0\ 0\ 0\,]^T$.

For the state equation (30), the switching function $\eta_2 = c_2x$ and the reaching law $\dot{\eta}_2 = c_2\dot{x} = -\varepsilon_2 sgn(\eta_2)\varepsilon_2 > 0$ are used to obtain the control law as follow,

$$u_W(t) = -(c_2B_1)^{-1}[c_2Ax(t) + c_2H\hat{d}(t) + \varepsilon_2 sgn(\eta_2)] \tag{31}$$

The corrected angular rotor speed ω_W can be expressed as

$$\omega_W = (1 + \frac{u_W - \Delta P_g}{\Delta P_g})\omega = \frac{u_W}{\Delta P_g}\omega \tag{32}$$

From (6), the gearbox torque $T_w(\beta, V_w, \omega_W)$ [28] is deduced as the following equation

$$T_w(\beta, V_w, \omega_W) = \frac{C_p(\lambda, \beta)V_w^3\rho\alpha}{2\omega_W} \tag{33}$$

where $\alpha = \pi R^2$. The accurate state equation of WTG model is hardly established because of its strong nonlinearity. Therefore, the linear state space model can be obtained by Taylor series expansion around the appropriate operation point. The high order terms are ignored, $T_w(\beta, V_w, \omega_W)$ is calculated at rated operation $(\beta_{op}, V_{wop}, \omega_{op})$ as

$$\Delta T_w = \bar{A}\Delta\omega_W + \bar{B}\Delta\beta + \bar{C}\Delta V_w \tag{34}$$

where

$$\bar{A} = \frac{V_{wop}^2\rho\alpha}{2\omega_{op}}(R\frac{\partial C_p}{\partial\lambda} - \frac{V_{wop}}{\omega_{op}}C_p), \quad \bar{B} = \frac{V_{wop}^3\rho\alpha}{2\omega_{op}}\frac{\partial C_p}{\partial\beta_{op}},$$

$$\bar{C} = \frac{\rho\pi R^2}{2}(3C_p\frac{V_{op}^2}{\omega_{op}} - RV_{wop}\frac{\partial C_p}{\partial\lambda}), \quad \Delta\omega_W = \omega_W - \omega_{op},$$

$\Delta\beta = \beta - \beta_{op}$ and $\Delta V_w = V_w - V_{wop}$.

The WTG [29] can be written as

$$J\frac{d\omega_W}{dt} = T_w - \gamma T_g - \varsigma\omega_W \tag{35}$$

where T_g is generator torque, γ is gear speed ratio, ς is viscous friction coefficient which can be ignored. Substitute (34) into (35) at rated operation point, then the state space equation is given as

$$\Delta\dot{\omega}_W = \frac{\bar{A}}{J}\Delta\omega_W + \frac{\bar{B}}{J}\Delta\beta + \frac{\bar{C}}{J}\Delta V_w \tag{36}$$

where $\Delta\omega_W$ is state variable, $\Delta\beta$ is control input, ΔV_w is disturbance, $\bar{A}$, $\bar{B}$, $\bar{C}$ are constant.

Traditional PI PAC may have long regulation time and large overshoot under randomness and volatility operation

case. So SM PAC is proposed for WTG system because of its quick response and robustness [26].

The SM LFC control includes two relatively independent parts of the SM surface for the desired performance and the control law for the system stability.

The switching function of sliding surface is defined as

$$\eta_2 = c_2 \Delta\omega_W \tag{37}$$

where c_1 is constant value.

The SM reaching law is selected as

$$\dot{\eta}_2 = c_2 \Delta\dot{\omega}_W = -\varepsilon_2 sgn(\eta_2)\varepsilon_2 > 0 \tag{38}$$

where ε_1 is positive constant, $sgn(\eta_1)$ is sign function.

Substitute (32), (38) into (36), the SM PAC can be derived as

$$\Delta\beta = -\frac{\left[J\varepsilon_2 sgn(\eta_2) + \bar{A}(\frac{u_W}{\Delta P_g}\omega - \omega_{op}) + \bar{B}\Delta V_w\right]}{\bar{C}} \tag{39}$$

In order to prove the WTG system stability with the designed SM PAC (39), the Lyapunov function is selected as

$$V_2 = \frac{1}{2}\eta_2^2 \tag{40}$$

Take the derivative of Lyapunov function (40) as,

$$\dot{V}_2 = \eta_2\dot{\eta}_2 = -\eta_2\varepsilon_2 sgn(\eta_2) \le 0 \tag{41}$$

Based on the analysis, the WTG system is stable by the designed SM PAC.

IV. COORDINATION CONTROL STRATEGY OF ISOLATED MICRO-GRID

The proposed coordination control strategy based on SM PAC and SM LFC is applied for the isolated micro-grid, the control strategy structure block diagram is shown in Fig.2.

From Fig.2, the coordination control strategy is consisted of SM LFC, SM PAC and RBF NNOA. SM LFC is designed for frequency adjustment which can improve the robustness for practical micro-grid with fluctuation renewable energy and variable load source. The WTG can be regulated by the designed SM PAC. The WTG system and the DG system can work together to improve the microgrid stability. The control precision of the system is further improved by using the RBF NNAO to obtain load estimation value.

The proposed comprehensive coordination strategy can be described and compared as following Table 1.

From Table 1, Eight different coordination strategies are given which include different control for WTG system, DG system and load, respectively. The proposed control strategy is composed of SM PAC for WTG side, SM LFC for DG side, RBF NNAO for load side. The closed loop control has been compensated between the WTG system and the DG system. The SM method is used to design the control which can improve the system robustness for the uncertainties and random disturbances affection. The adaptive observer is applied to estimate load value which can improve the control accuracy. The closed loop control can improve the system stability. Some of the strategies in Table 1 may be tested through simulation in the next section, which can show the advantages of the proposed strategy.

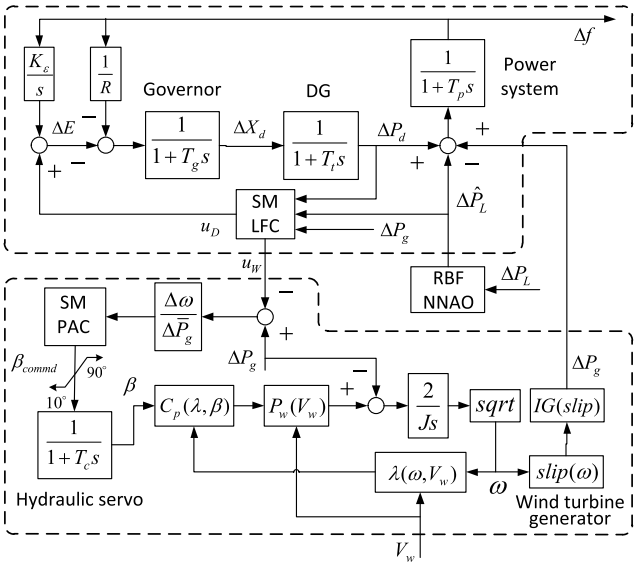

FIGURE 2. The control structure diagram.

TABLE 1. Different coordination strategy.

Coordination Strategy	DG System	WTG System	Load	Loop
Strategy 1	PI LFC	MPPT control	RBF NNAO	Open Loop
Strategy 2	PI LFC	PI PAC	RBF NNAO	Open Loop
Strategy 3	PI LFC	SM PAC	RBF NNAO	Open Loop
Strategy 4	SM LFC	MPPT control	RBF NNAO	Open Loop
Strategy 5	SM LFC	PI PAC	RBF NNAO	Open Loop
Strategy 6	SM LFC	PI PAC	RBF NNAO	Close Loop
Strategy 7	SM LFC	SM PAC	RBF NNAO	Open Loop
Proposed Strategy	SM LFC	SM PAC	RBF NNAO	Close Loop

V. EXPERIMENT RESULTS AND ANALYSIS

To verify the effectiveness of the proposed coordination control strategy, the controller hardware-in-the-loop (CHIL) experiments are carried out in a real-time digital simulator (RTDS) platform. The schematic diagram of the CHIL test bed setup is shown in Fig. 3, where a RTDS facility for real-time modeling, a digital-signal-processor (DSP) controller for control firmware verifications, and a RSCAD for monitoring/control are drawn. To simplify the overall CHIL configurations and focus on the verifications of the proposed coordination control, the WTG, DG and load together with the associate control system are simulated in the real-time simulator with the sampling time of 50μs, whereas the

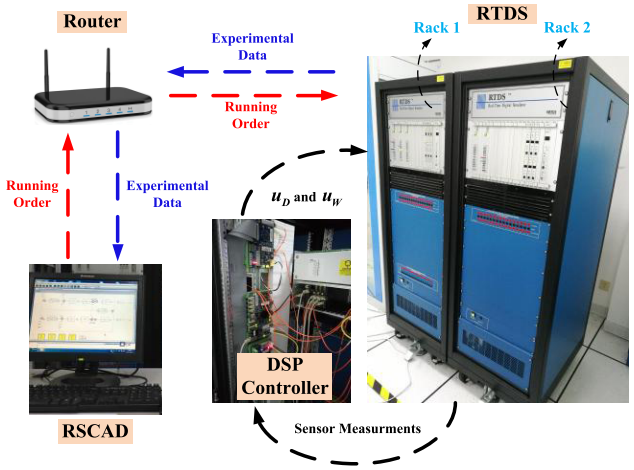

FIGURE 3. The experiment structure diagram.

TABLE 2. Simulation parameters.

Parameter	value	Parameter	value
R	14	R_1	0.00397
J	62993	X_1	0.00376
ρ	1.23	R_2	0.00443
P_g	275 (0.5 p.u.)	X_2	0.05340
V	230.94	T_c	1
$-1/T_p$	-0.0665	K_p/T_p	8
$-1/T_t$	-3.663	$-1/T_g$	-13.736
R_{tr}	2.00233	ΔK_ε	0.6
L_1	22.5345	L_2	19.5563
L_3	17.4995	L_4	-24.2435

SM-LFC control algorithm and the adaptive observer are programmed in the hardware DSP controller. The output signals of the RTDS are the changing rate of load, DG, and WTG powers, which are subsequently sent to the DSP controller. To form up a close-loop between real-time modeling and controller hardware, the outputs of the DSP controller are u_D and u_W, which are eventually feedback to the DG and WTG control systems for frequency compensation in the real-time models. By setting up the complete CHIL testbed, five cases are studied to validate the proposed control strategy and the results are analyzed in the following sub-sections.

For the isolated hybrid micro-grid, the capacities of wind power, DG and load are 380 kW, 275 kW, and 480 kW, respectively. The parameters of isolated hybrid micro-grid are given in Table 2. The per unit values of the experiment results can be seen in the following figures. The power reference is about 550 kW and the frequency reference is about 50 Hz.

There are five cases to test the proposed coordination control strategy as in Table 1. In case 1, WTG system is operated under normal MPPT mode and the DG system is controlled by the traditional PI control. Case 2 shows two control methods that SM only applied to WTG system or DG system. In case 3, the SM LFC for DG system and SM PAC for WTG system are used. Then the

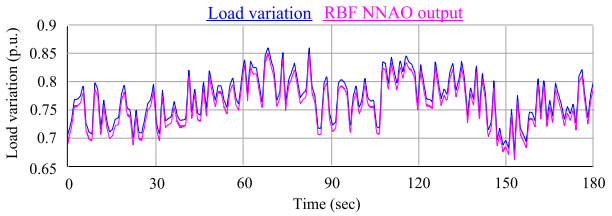

FIGURE 4. The load variation and output of RBF NNAO.

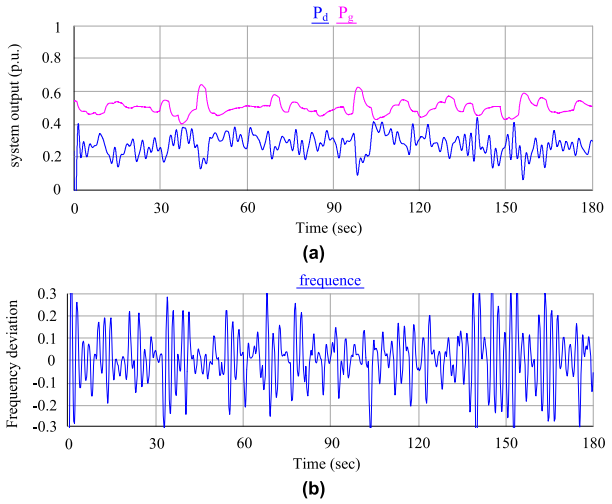

FIGURE 5. The simulation results without SM control frequency regulation. (a) output power of the DG system and WTG system, (b) frequency deviation.

proposed coordinated control strategy with intelligent load estimation is used to restrain the frequency deviation in case 4. In case 5, the proposed coordinated control strategy is tested under step load disturbance and step wind speed disturbance, respectively.

The load variation is shown in Fig. 4. The actual load value and the estimated value by RBF NNAO is shown as Fig.4. Here, the simulation time is 180s, neuron is 6, F_1 is 10000, k_1 is 0.001.

From the simulation results, the load variation can be estimated precisely by correcting RBF NNAO weight timely through adaptive algorithm.

A. CASE 1

In this case, WTG system operates under normal MPPT mode. The DG system is controlled by the traditional PI control for secondary frequency regulation.

From the RTDS results in Fig 5, the renewable resource can be adequately used, however, the frequency deviation exceeds ±0.2 Hz because of renewable energy and load fluctuation, sometimes it may large over, which can affect the power quality seriously.

B. CASE 2

In this case, the SM method is only applied to WTG system or DG system. The output power of DG system and

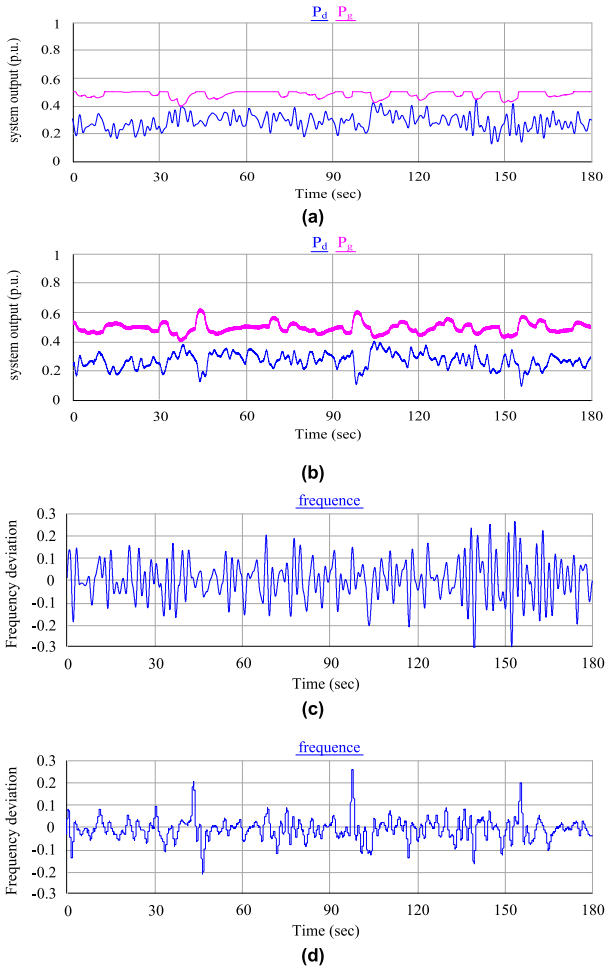

FIGURE 6. (a) output power (WTG system with SM PAC and DG system with traditional PI LFC), (b) output power (WTG system with traditional PI control and DG system with SM LFC), (c) frequency deviation (WTG system with SM PAC and DG system with traditional PI LFC), (d) frequency deviation(WTG system with traditional PI PAC and DG system with SM LFC).

WTG system are shown as Fig 6 (a)-(b) with different control method. For the WTG system with SM PAC and the DG system with traditional PI LFC, frequency deviation is shown as Fig. 6 (c). For the WTG system with traditional PI control and the DG system with SM LFC, frequency deviation is shown as Fig 6 (d). The RTDS results show that case 2 has smaller frequency deviation and smoother than case 1. The frequency deviation is less than 0.2 Hz during most of the time, but sometimes it exceeds ±0.2 Hz. From Fig. 6 (c) and (d), frequency deviation is improved because the DG system with different LFC.

C. CASE 3

In this case, the double SM method is used for LFC and PAC design. WTG output power is smoother through using SM PAC. Renewable energy is still fully utilized because distributed energy is not involved in frequency management of isolated hybrid micro-grid. The simulation results are shown in Fig 7.

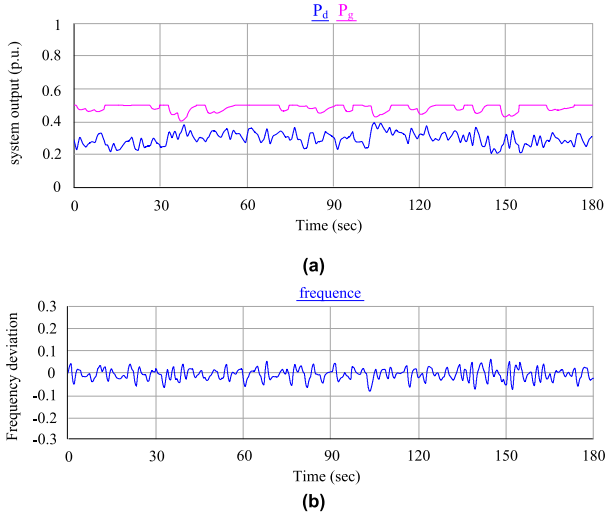

FIGURE 7. The simulations result with SM LFC and SM PAC. (a) output power of DG system and WTG system, (b) frequency deviation.

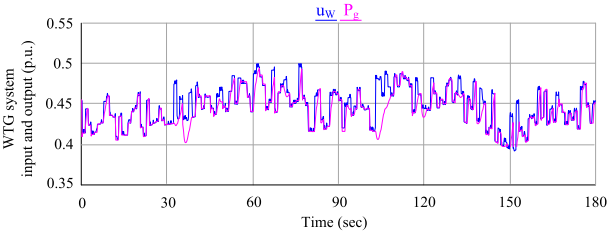

FIGURE 8. WTG system reference value and output power.

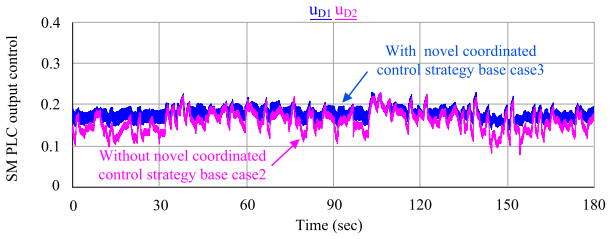

FIGURE 9. Control variable u_d by the LFC for the DG system.

From the RTDS results, frequency deviation is restrained within ±0.1 Hz by using SM LFC for DG system and SM PAC for WTG system. The output power fluctuation of DG system is smoother than in case 2. However, this control method does not make use of the wind energy taking part in the frequency adjustment.

D. CASE 4

From Case 3, the novel coordinated control strategy is proposed by taking advantage of intelligent load estimation for frequency deviation restrain. The SM PAC is designed for WTG system to smooth wind output power, and the reference value u_W of PAC is defined by SM LFC. The SM LFC is designed for DG system to restore system frequency through the secondary frequency regulation. The RTDS results

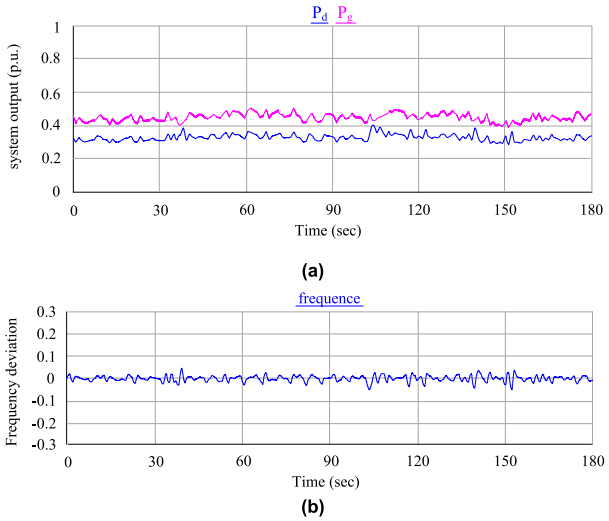

FIGURE 10. Output waveform with proposed coordinated control strategy based on intelligent load estimation (a) output power of WTG system and DG system, (b) frequency deviation.

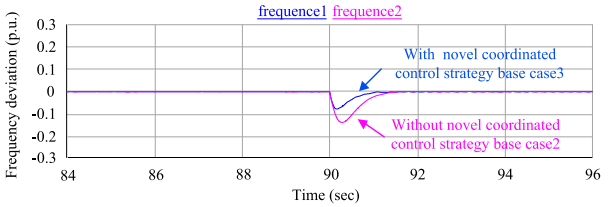

FIGURE 11. Frequency deviation with step load disturbance.

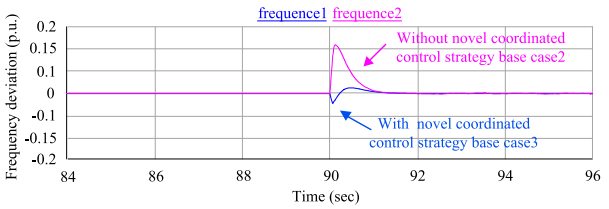

FIGURE 12. Frequency deviation with step wind speed disturbance.

are shown as Fig.8-10. It can be seen from Fig.8 that WTG system output power is smoother. From Fig.9, control variable u_D. for the DG system has smaller fluctuation. From Fig.10, output power of DG system and WTG system are smoother than the above cases. The frequency deviation is restrained within ± 0.1 Hz.

E. CASE 5

In order to further verify the advantage of the proposed coordinated control strategy, step load disturbance and step wind speed disturbance are tested in this case.

At $t = 90s$, the isolated hybrid micro-grid is disturbed by step load disturbance (0.1p.u.) and step wind speed disturbance (3 m/s) which is without and with the proposed coordinated control strategy. The RTDS results are shown as the following Figures.

From Fig.11-12, the frequency deviation has smaller fluctuation amplitude with the proposed coordinated control strategy.

VI. CONCLUSION

The coordinated control strategy is proposed to reduce frequency deviation and improve frequency control robustness for isolated hybrid micro-grid based on intelligent load estimation and SM method. Considering the load variation and the output power fluctuation of WTG, the RBF NNAO and the adaptive law are designed to improve the accuracy of the SM LFC and SM PAC. Different coordination operation cases are simulated by RTDS platform which show that the frequency deviation can be properly controlled within smaller range.

REFERENCES

[1] I. Poultangari, R. Shahnazi, and M. Sheikhan, "RBF neural network based PI pitch controller for a class of 5-MW wind turbines using particle swarm optimization algorithm," *ISA Trans.*, vol. 51, no. 5, pp. 641–648, 2012.

[2] Y. Oğuz, S. V. Üstün, I. Yabanova, M. Yumurtaci, and I. Güney, "Adaptive neuro-fuzzy inference system to improve the power quality of a split shaft microturbine power generation system," *J. Power Sources*, vol. 197, no. 1, pp. 196–209, 2012.

[3] A. Musyafa *et al.*, "Pitch angle control of variable low rated speed wind turbine using fuzzy logic controller," *Int. J. Eng. Technol.*, vol. 10, no. 5, pp. 21–24, 2010.

[4] M. Heidari, "Intelligent control for the variable-speed variable-pitch wind energy system," *Iranian J. Elect. Electron. Eng.*, vol. 13, no. 3, pp. 278–286, 2017.

[5] K. Boulâam and A. Boukhelifa, "Output power control of a wind energy conversion system based on a doubly fed induction generator," in *Proc. Int. Renew. Sustain. Energy Conf.*, Ouarzazate, Morocco, Mar. 2013, pp. 292–297.

[6] H. Bevrani, *Robust Power System Frequency Control*. New York, NY, USA: Springer, 2009.

[7] S. Saxena and Y. V. Hote, "Decentralized PID load frequency control for perturbed multi-area power systems," *Int. J. Elect. Power Energy Syst.*, vol. 81, pp. 405–415, Oct. 2016.

[8] W. Tan, "Unified tuning of PID load frequency controller for power systems via IMC," *IEEE Trans. Power Syst.*, vol. 25, no. 1, pp. 341–350, Feb. 2010.

[9] S. Sönmez and S. Ayasun, "Stability region in the parameter space of PI controller for a single-area load frequency control system with time delay," *IEEE Trans. Power Syst.*, vol. 31, no. 1, pp. 829–830, Jan. 2016.

[10] G. T. C. Sekhar, R. K. Sahu, A. K. Baliarsingh, and S. Panda, "Load frequency control of power system under deregulated environment using optimal firefly algorithm," *Int. J. Elect. Power Energy Syst.*, vol. 74, pp. 195–211, Jan. 2016.

[11] N. Chuang, "Robust H_∞ load-frequency control in interconnected power systems," *IET Control Theory Appl.*, vol. 10, no. 1, pp. 67–75, Jan. 2016.

[12] Y. Zhang, X. Liu, and B. Qu, "Distributed model predictive load frequency control of multi-area power system with DFIGs," *IEEE/CAA J. Autom. Sinica*, vol. 4, no. 1, pp. 125–135, Jan. 2017.

[13] X. Liu, Y. Zhang, and K. Y. Lee, "Coordinated distributed MPC for load frequency control of power system with wind farms," *IEEE Trans. Ind. Electron.*, vol. 64, no. 6, pp. 5140–5150, Jun. 2017.

[14] G. Ray, S. Dey, and T. K. Bhattacharyya, "Multi-area load frequency control of power systems: A decentralized variable structure approach," *Electr. Power Compon. Syst.*, vol. 33, no. 3, pp. 315–331, 2004.

[15] G. Rinaldi, M. Cucuzzella, and A. Ferrara, "Third order sliding mode observer-based approach for distributed optimal load frequency control," *IEEE Control Syst. Lett.*, vol. 1, no. 2, pp. 215–220, Oct. 2017.

[16] G. Magdy, E. A. Mohamed, G. Shabib, A. A. Elbaset, and Y. Mitani, "SMES based a new PID controller for frequency stability of a real hybrid power system considering high wind power penetration," *IET Renew. Power Gener.*, vol. 12, no. 11, pp. 1304–1313, 2018.

[17] P. Manjarres and O. Malik, "Frequency regulation by fuzzy and binary control in a hybrid islanded microgrid," *J. Mod. Power Syst. Clean Energy*, vol. 3, no. 3, pp. 429–439, 2015.
[18] N. Mendis, K. M. Muttaqi, and S. Perera, "Active power management of a super capacitor-battery hybrid energy storage system for standalone operation of DFIG based wind turbines," in *Proc. IEEE Ind. Appl. Soc. Annu. Meeting*, Las Vegas, NV, USA, Oct. 2012, pp. 1–8.
[19] A. Ghafouri, J. Milimonfared, and G. B. Gharehpetian, "Fuzzy-adaptive frequency control of power system including microgrids, wind farms, and conventional power plants," *IEEE Syst. J.*, vol. 12, no. 3, pp. 2772–2781, Sep. 2018.
[20] M. Datta, T. Senjyu, A. Yona, T. Funabashi, and C.-H. Kim, "A frequency-control approach by photovoltaic generator in a PV–diesel hybrid power system," *IEEE Trans. Energy Convers.*, vol. 26, no. 2, pp. 559–571, Jun. 2011.
[21] S. A. Papathanassiou and M. P. Papadopoulos, "Dynamic characteristics of autonomous wind–diesel systems," *Renew. Energy*, vol. 23, no. 2, pp. 293–311, 2001.
[22] Y. Wang, R. Zhou, and C. Wen, "Robust load-frequency controller design for power systems," *IEE Proc. C (Generat., Transmiss., Distrib.)*, vol. 140, no. 1, pp. 11–16, Jan. 1993.
[23] T. Senjyu, R. Sakamoto, N. Urasaki, T. Funabashi, H. Fujita, and H. Sekine, "Output power leveling of wind turbine Generator for all operating regions by pitch angle control," *IEEE Trans. Energy Convers.*, vol. 21, no. 2, pp. 467–475, Jun. 2006.
[24] J. Pahasa and I. Ngamroo, "Coordinated control of wind turbine blade pitch angle and PHEVs using MPCs for load frequency control of microgrid," *IEEE Syst. J.*, vol. 10, no. 1, pp. 97–105, Mar. 2016.
[25] H. Bevrani and P. R. Daneshmand, "Fuzzy logic-based load-frequency control concerning high penetration of wind turbines," *IEEE Syst. J.*, vol. 6, no. 1, pp. 173–180, Mar. 2012.
[26] C. Wang, Y. Mi, Y. Fu, and P. Wang, "Frequency control of an isolated micro-grid using double sliding mode controllers and disturbance observer," *IEEE Trans. Smart Grid*, vol. 9, no. 2, pp. 923–930, Mar. 2018.
[27] B. Chen, H. Zhang, and C. Lin, "Observer-based adaptive neural network control for nonlinear systems in nonstrict-feedback form," *IEEE Trans. Neural Netw. Learn. Syst.*, vol. 27, no. 1, pp. 89–98, Jan. 2016.
[28] X. Liu, P. Wang, and P. C. Loh, "A hybrid AC/DC microgrid and its coordination control," *IEEE Trans. Smart Grid*, vol. 2, no. 2, pp. 278–286, Jun. 2011.
[29] S. Li and J. Li, "Output predictor-based active disturbance rejection control for a wind energy conversion system with PMSG," *IEEE Access*, vol. 5, pp. 5205–5214, 2017.

Authors' photographs and biographies not available at the time of publication.